Microstructure, decomposition, and crystallization in $Zr_{41}Ti_{14}Cu_{12.5}Ni_{10}Be_{22.5}$ bulk metallic glass

Wei-Hua Wang*
Institute of Physics, Chinese Academy of Sciences, 100080 Beijing, China
and Hahn-Meitner-Institut, Glienicker Strasse 100, D-14109 Berlin, Germany

Q. Wei and S. Friedrich
University Potsdam, Institute Berufspädagogik, Golm, D-14467 Potsdam, Germany
(Received 9 July 1997; revised manuscript received 12 November 1997)

The microstructure as well as the decomposition and crystallization of the $Zr_{41}Ti_{14}Cu_{12.5}Ni_{10}Be_{22.5}$ bulk metallic glass (MG) has been investigated. The effects of the decomposition on the subsequent crystallization are determined. Reduced density function analyses for the MG, and the decomposition and crystallization in the MG have been made by means of electron-diffraction intensity measurement with imaging plate to determine the local atomic structure and its development in the course of the decomposition and crystallization. The microstructural characteristics of the MG are obtained demonstrating the difference between the bulk MG and conventional MG. The origin of the large glass forming ability of the alloy and the effect of the phase separation on the crystallization are discussed based on the obtained local atomic structural information of the MG. [S0163-1829(98)01914-6]

I. INTRODUCTION

Johnson *et al.*[1–6] have developed a unique multicomponent glass forming system $Zr_{41}Ti_{14}Cu_{12.5}Ni_{10}Be_{22.5}$ with a wide supercooled liquid region (SLR). The metallic glass (MG), which shows the best glass forming ability (GFA) known so far, can be obtained at various shapes and sizes even by the conventional casting process at a low cooling rate. This brings bulk MG close to technical applicability. The phase separation has been discovered in the supercooled liquid state of the MG, and intensive attention has been paid to the decomposition phenomenon and much effort has been devoted to this work.[7–13] The low cooling rate for the formation of the MG allows one to observe the phase separation taking place below a miscibility gap in the SLR. Field ion microscopy with atom probe (FIM/AP) investigation revealed that the MG decomposed into a Be-rich and a Ti-rich amorphous phase. Be and Ti show clear anticorrelated concentration fluctuations; Zr, Cu, Ni do not participate significantly in the decomposition of the supercooled liquid melt.[10,11] However, up to now, the effects of the decomposition on the subsequent crystallization is a controversial question,[10–13] because the adequate experimental data concerning the effects have not been achieved, and the different experiments lead to contradicting results. The microstructural characteristics of the MG have not been investigated because of the complex chemistry of the alloy, the microstructural characteristics should have close relation with the high GFA and the decomposition of the MG. The local atomic structural development during the phase separation and crystallization is still not clear. Reduced density function (RDF), $G(r)$, evaluated by diffraction method, is an effective way to describe the local atomic structure of a MG. It can provide general information concerning the degree of structural randomness, the average atomic correlation distances, and the average nearest-neighbor coordination numbers. This information is very important for understanding the origin of the large GFA, the decomposition, and the crystallization phenomena in the MG. However, the local atomic structure in the nearest-neighbor region is not determined by the conventional diffraction method, because the alloy system consists of five elements with greatly different atomic sizes. Electron-diffraction intensity analysis with imaging-plate (IP) technique is one way to overcome this difficulty, and this method has been developed for obtaining RDF from amorphous materials in recent years.[14–16] It has a number of advantages over x-ray and neutron-diffraction techniques for the structural investigation of amorphous materials. The most important of these is the large scattering cross section that permits rapid data collection with good statistics. Secondly, the small wavelength compared to x-ray and neutron-diffraction techniques allows the collection of data to obtain a large value of wave number, because the wave number is inversely proportional to the wavelength, and then achieves good resolution in real space. Additionally, the diffraction intensity can be parallel and recorded at all scattering angles simultaneously, and the structural information can be obtained from small chosen regions of the specimen. The development of the ''imaging plate'' technique[17] enables one to measure electron-diffraction intensity correctly because IP is of a wide dynamic range and has excellent linearity for the electron intensity. In this work, the decomposition, crystallization, as well as the influence of decomposition on the crystallization in the $Zr_{41}Ti_{14}Cu_{12.5}Ni_{10}Be_{22.5}$ MG, are studied. Electron-diffraction intensity analyses with the help of IP are applied for obtaining the RDF from the MG. The local atomic structural development during the decomposition and crystallization of the glass is presented. The large GFA and the effects of the decomposition on the crystallization of the alloy are discussed by using the information of the local atomic structure. An additional motivation for the study is simply to provide local structural information concerning the multicomponent bulk MG, in order to determine how it compares structurally to other conventional MG.

II. EXPERIMENTAL AND ELECTRON-DIFFRACTION INTENSITY ANALYSIS THEORY

Amorphous alloy ingots, with nominal composition $Zr_{41}Ti_{14}Cu_{12.5}Ni_{10}Be_{22.5}$, were prepared from a mixture of the elements of purity ranging from 99.9% to 99.99% by induction melting under a Ti-gettered Ar atmosphere. The ingots were remelted in a sealed silica tube under pure Ar atmosphere and were subsequently water quenched, resulting in a cylindrical rod with a diameter of 12 mm. The details of the preparation process are described in Ref. 11. The homogenous glass nature of the MG was previously approved by x-ray diffraction (XRD),[3,9] differential scanning calorimeter (DSC) (Refs. 3 and 11), and small angle neutron scattering (SANS).[10,13] DSC results show that the MG exhibits a significantly large SLR, ΔT ($\Delta T = T_x - T_g$ is 50 K), which is defined as the difference of the glass transition temperature T_g (623 K) and the onset temperature of the crystallization event T_x (673 K). The cross-sectional thin foils cut from the middle of the MG rod were investigated by transmission electron microscopy (TEM). When the specimens were annealed, each of them was heated up to the desired temperature using a rate of about 10 K/min, and cooled down to about 20 K/min to ensure the same thermal history for all specimens. TEM experiments were performed in a Philips EM400 operating at 120 kV. Selected area electron-diffraction intensities were recorded on the IP with the same exposure time of 0.5 s under the same camera length of 450 cm (corrected using a TlCl reference particle). The intensity record was divided into 256^2 grey levels. The details of the TEM experimental procedure are referred to in Ref. 18. The recorded intensities were digitized by using a computer, followed by the RDF analysis.

A reduced intensity function is defined by[19,20]

$$F(Q) = [I(Q) - N\langle f^2\rangle]Q/N\langle f\rangle^2 = \int_0^\infty [\rho(r) - \rho_0]4\pi r \sin(Qr)dr, \quad (1)$$

where $I(Q)$ is elastic scattering intensity, and r is the modulus of the position vector of the atom. $Q = 4\pi \sin\theta/\lambda$ (θ is the half scattering angle and λ the electron wave length), $\rho(r)$ is the radial number density function

$$\langle f\rangle^2 = \left(\sum_i N_i f_i\right)^2/N^2 \text{ and } \langle f^2\rangle = \sum_j N_j f_j^2/N,$$

where N_i and f_i correspond to the atomic number and atomic scattering function of the element i, respectively. $N = \Sigma_i N_i$, ρ_0, the average density of the sample. The value of N is chosen to minimize the oscillations in RDF curves at small r.

Then the reduced density function $G(r)$ can be yielded by the Fourier inversion

$$G(r) = 4\pi r[\rho(r) - \rho_0] = 8\pi \int_0^\infty F(Q)\sin(Qr)dQ. \quad (2)$$

$G(r)$ describes the deviation of $\rho(r)$ from ρ_0 in the sample, the maxima in $G(r)$ give the most probable distances between atoms of types i and j.[20]

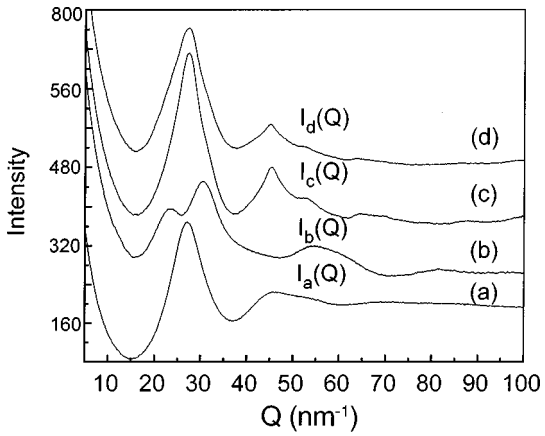

FIG. 1. Electron-diffraction intensities of the $Zr_{41}Ti_{14}Cu_{12.5}Ni_{10}Be_{22.5}$ MG at different annealing temperatures measured by an imaging plate: (a) as-quenched state; (b) annealed in 623 K for 62 h; (c) annealed at 623 K for 15 h and then annealed at 653 K for 1 h; (d) annealed at 673 K for 1 h.

III. RESULTS

A. Electron-diffraction intensity analysis

We analyzed the intensity data assuming that the diffraction pattern contains only an elasticity scattering electron, because the elastic intensity change with scattering angle is difficult to measure correctly. This assumption does not have significant influence on obtaining the local atomic structure information of the amorphous alloy, because the integrated areas and the positions of the RDF peaks took only slightly different values when analyzed without the intensity correction for the inelastic scattering.[16] The effects of the multiple scattering depend upon the specimen thickness D and the elastic mean-free path. They can be minimized either by choosing parameters D and the electron energy such that multiple scattering is negligible.[14] In our experiments, the effects have been minimized by the use of thin specimens, $D < 50$ nm. An amorphous structure model of $Pd_{75}Si_{25}$ with a thickness of 10 nm was created by computer and the multiple scattered intensity was compared with a kinematical intensity: no appreciable difference between the calculated kinematical and multiple scattered intensity was observed. The reliability of the method of the electron-diffraction intensity analysis with IP has been checked against the known crystalline and amorphous structures such as Pt and amorphous Si, and excellent agreement with the RDF reconstructed from the diffraction data for these structures was obtained.[14,16,17]

Average intensities $I(Q)$ were obtained up to the scattering vector $Q = 200$ nm^{-1}. The electron-diffraction curves of the MG at various annealing temperatures are presented in Fig. 1. For the as-quenched sample, the curve $I_a(Q)$ in Fig. 1(a) exhibits a broad maximum peak followed by another of lesser intensity that is characteristic of a single amorphous structure: no peaks indicative of the presence of crystalline phase could be detected. Figure 1(b) shows the electron-diffraction curve $I_b(Q)$ of the MG annealed at 623 K for 62 h. The first peak splits into two broad peaks, and no sharp diffraction peaks form in the process. The TEM dark field micrograph imaged by the light of the outer ring shows that the nanosized amorphous clusters of one phase are visible in the bright contrast. The results indicate that the MG sepa-

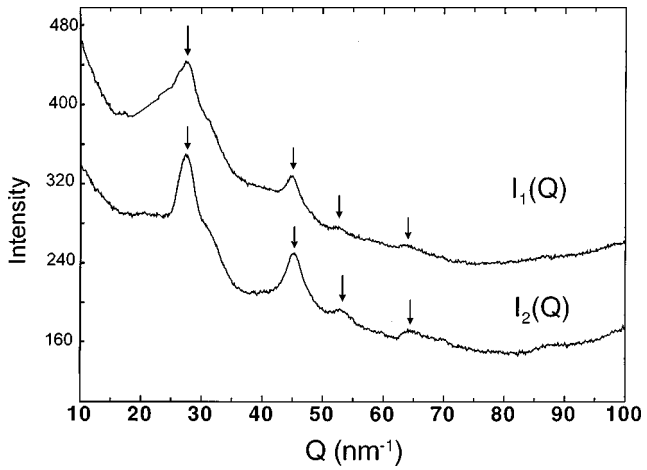

FIG. 2. Difference $I_1(Q)$, $I_2(Q)$ representing the changes in the electron-diffraction patterns of the $Zr_{41}Ti_{14}Cu_{12.5}Ni_{10}Be_{22.5}$ MG induced by the partial crystallization with and without preceding decomposition, respectively.

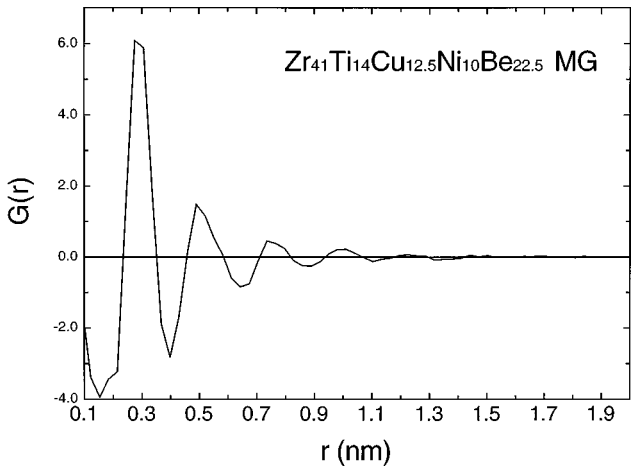

FIG. 3. RDF profile of the $Zr_{41}Ti_{14}Cu_{12.5}Ni_{10}Be_{22.5}$ MG.

rates into two different amorphous phases. The decomposed phases are Be-rich and Ti-rich amorphous phases.[13] A microstructure of the precipitates of the amorphous phase with a radius of up to 3 nm embedded in the second amorphous phase matrix was also found by SANS.[10] The phase separation process in the MG was confirmed by XRD (Ref. 21) and FIM/AP methods.[3,9]

To determine the influence of the decomposition on the crystallization behavior, the MG specimens were treated with different annealing conditions. One was isothermal annealed at 623 K for 15 h, and then additionally annealed at 653 K for 1 h. The isothermal annealed at 623 K was performed to cause a decomposition of the glass prior to the crystallization, and then to exhibit the effects of the decomposition on the subsequent crystallization (i.e., a preceding decomposition treatment). The diffraction curve $I_c(Q)$ of the specimen is shown in Fig. 1(c). The first peak becomes sharper, and represents the superimposition of the formed crystalline phases and the remaining amorphous phase. The second peak splits and shows the Bragg reflection of the crystalline phase. Other sharp diffraction peaks in the higher angle range have also been found. The results indicate the MG with the preceding decomposition crystallizes in the SLR. The dark field TEM picture shows the specimen with preceding decomposition has finer and denser nanoscale crystallites, the median crystalline size is 2 nm. The diffraction curve $I_d(Q)$ of the sample that is directly annealed near T_x (673 K) for 1 h is shown in Fig. 1(d). A superimposition of the diffuse amorphous peak and the sharp crystalline peaks arising from partial crystallization can be seen in the curve. The dark field TEM picture shows sparse and various sizes of the crystallites distributed randomly in the amorphous matrix. The average size is 3.5 nm.

To evaluate and compare the crystallization behavior of the two partially crystallized samples with and without the preceding decomposition, the intensity data for the MG was subtracted from that of the two crystallized samples. The resulting $I_1(Q)=I_c(Q)-I_a(Q)$ and $I_2(Q)=I_d(Q)-I_a(Q)$ are presented in Fig. 2. The two curves have completely corresponding Bragg's peaks, which means the crystallized phases in both cases are identical. However, the sample with the preceding decomposition has relatively stronger Bragg peaks. The diffraction intensities analyses confirm that the crystallization in the MG is affected by the preceding decomposition. The preceding decomposition promotes nucleation in the MG and thermally destabilizes the MG. The different crystallite size distributions in the two specimens are a result of the different nucleation processes. The crystallites in the specimen without preceding decomposition are formed by a homogeneous nucleation by a composition fluctuation from the initial homogeneous alloy. In contrast, the crystallites in the specimen with preceding decomposition are formed by heterogeneous nucleation processes. The interfaces between the decomposed phases provide the nucleation sites and facilitate the nucleation of the crystalline phases. This leads to the crystallization of the MG at lower temperature. The results also indicate that the crystallization in the MG can undergo different paths to the crystallization. The MG can directly crystallize by nucleation and growth from the initial homogeneous MG, or decompose into two amorphous phases; the decomposed phases crystallize at relatively lower temperature.

B. Local structure of the metallic glass

The RDF profiles are computed by the Fourier transformation of $I(Q)$ truncated at $Q_{\max}=200\ \mathrm{nm}^{-1}$. The range of Q in Eq. (1) should be theoretically infinite, but in practice Q is finite. The termination of the integration leads to termination error. However, electron diffraction allows the collection of Q to be a large value: the integration is accurate enough for the value of $Q_{\max}$.[20] An artificial damping, $\exp(-0.002Q^2)$, is also applied to the structure factor to minimize the termination error.[19] The lower limit of Q is $0.03\ \mathrm{nm}^{-1}$ in all Fourier inversions. The small-angle scattering due to the finite size of the scattering volume has been ignored in the derivation of $G(r)$, because the Fourier inversion of the small-angle scattering results in an oscillation in the $G(r)$ at small r. The corresponding RDF curve of the MG is given in Fig. 3. The RDF profile shows a strong peak at a mean distance of 0.28 nm and progressively weaker peaks at 0.48 and 0.72 nm. The first peak represents a mainly nearest-neighbor correlation of the atomic pair Zr-Be in the MG. $G(r)$ is dominated by Zr-Be pairs, because the pair has

relatively larger weight factors.[19] The MG exhibits a broad radial distribution of the first nearest neighbor that begins at 0.23 nm and ends at 0.36 nm, which is much broader than that of the conventional MG. The broad peak is attributed to the complex chemistry and the larger atomic difference between the Zr and Be atomic radius r_{Zr} and r_{Be} in the MG ($r_{Be}/r_{Zr}=0.70$), it may correspond to other nearest-neighbor atomic pairs, for example, the Zr-Ni pair and the Cu-Ti pair. The broadness of the peak also suggests that the MG possesses a complex and close-packed atomic environment. The second peak has no obvious separation, which is the characteristic of a conventional MG, and the feature of the RDF is analogous to that of a liquid phase. This means that the multicomponent MG has a homogeneously mixed atomic configuration corresponding to a much higher degree of a dense random-packed structure with a lower fraction of free volume. This structural characteristic, which is distinct from conventional MG, has also been found in other multicomponent MG systems.[22,23] The attempt to calculate the coordination numbers of the elements was unsuccessful, and it gave a too high coordination number to be reasonable, because the first peak corresponds to several neighboring atomic pairs. Up to now, the composition and the structure of the crystallized compounds of the MG have not been determined, because of the chemistry complexity and the difficulty of detecting Be by XRD and TEM in the MG. It is difficult to perform a comparative analysis of a complex unknown glass structure by checking the results against some known corresponding crystalline structures so as to quantitatively determine the coordination number of the MG. However, the local structure changes induced by the decomposition and crystallization of the MG can be found by evaluation of the evolution of the position (corresponds to atom pair) and area (corresponds to the change of the coordination number of the atom pair) of the first peak of RDF curves. The shape of the RDF curve can also provide some additional information about the local structure changes. The RDF profile of the MG is similar to that of the same specimen studied by neutron diffraction,[24] suggesting that the IP intensity measurement method is quite helpful and reliable in analyzing the electron-diffraction intensities.

C. The development of the local structure in decomposition and crystallization

In Fig. 4 the RDF curves corresponding to Figs. 1(a)–1(d) are denoted by $G_a(r)$, $G_b(r)$, $G_c(r)$, and $G_d(r)$, respectively. Figure 4(a) shows the RDF profile of the as-quenched MG. The RDF profile of the MG after complete decomposition is shown in Fig. 4(b). The first peak in the profile shows a splitting into two subsidiary peaks with average distance $r=0.32$ nm and $r=0.24$ nm. The former corresponds to the interatomic distance of the Zr-Zr pair ($r=0.318$ nm), and the latter Be-Cu pair ($r=0.239$ nm) or Be-Ni pair ($r=0.235$ nm). This splitting is a consequence of the decomposition in the MG. The different first nearest-neighbor radial density distributions obtained in the decomposed MG demonstrate the different local structure of the decomposed phases. This suggests that the decomposition has a significant affect on the chemical and topological configurations of the MG. The MG has decomposed into two amorphous

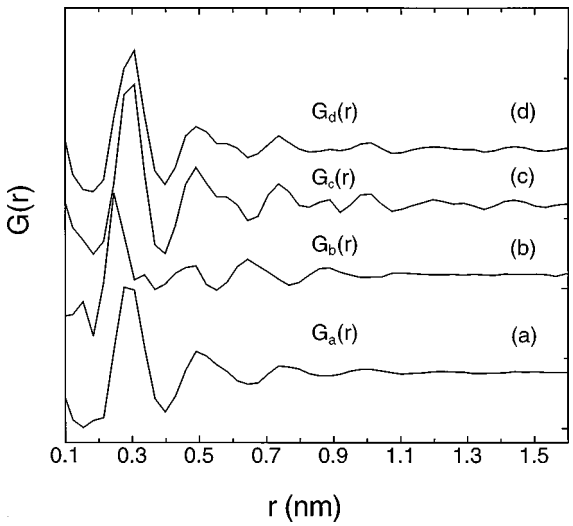

FIG. 4. RDF profiles of the $Zr_{41}Ti_{14}Cu_{12.5}Ni_{10}Be_{22.5}$ MG treated at different annealing conditions: (a) as-quenched state; (b) annealed at 623 K for 62 h; (c) annealed at 623 K for 15 h and then annealed at 653 K for 1 h; (d) annealed at 673 K for 1 h.

phases with different short-range orders and compositions. The atomic local environment in the MG is largely rearranged in the phase separation process. Figures 4(c) and 4(d) show the RDF profiles for the samples annealed with and without preceding decomposition, respectively. The peaks of $G_c(r)$ and $G_d(r)$ are higher and sharper than those in $G_a(r)$. The functions represent structural changes introduced into the initial MG by crystallization. The position of the first peak (representing the Zr-Be atom pair) in the RDF profiles of the two annealed samples shifts to 0.3 nm, the area of the first peak increases compared with that of the as-quenched MG. This means the Zr-Be correlation distance and its average coordination number are changed after crystallization. The results also indicate that the large atom redistribution is required for crystallization. It is also found that several additional peaks appear in the $G(r)$ profiles of the partial crystallization samples, which indicate some locally ordered regions are formed in the samples. The additional features observed in $G(r)$ at a distance up to 1.5 nm, may arise from small clusters that form during the crystallization. The large changes in RDF between the MG and the crystallized MG, including the average nearest-neighbor distance of the Zr-Be atomic pair, the coordination number, as well as the feature of the $G(r)$ profiles, reveal that the local atomic structure of the MG is markedly changed by crystallization. This demonstrates that the large local structural differences between the MG and its corresponding crystallized phases exist. To accentuate the differences and show the local structural development introduced by crystallization, the function $G_a(r)$ has been subtracted from $G_c(r)$ and $G_d(r)$. Figure 5 shows the functions $G_{c-a}(r)$ and $G_{d-a}(r)$ that represent local structural changes induced by crystallization. One can see from the figure that $G_{c-a}(r)$ and $G_{d-a}(r)$ have no corresponding peaks to $G_a(r)$: the peaks around $r=1.5$ nm also become visible. The peaks in both of the $G_{c-a}(r)$ and $G_{d-a}(r)$ for the crystalline case tend to be smaller than that of $G_a(r)$ for the MG case. The differences in peak positions and area for $G_a(r)$ compared with $G_{c-a}(r)$ and $G_{d-a}(r)$ confirm a dramatic change of the local structure with respect to that of the

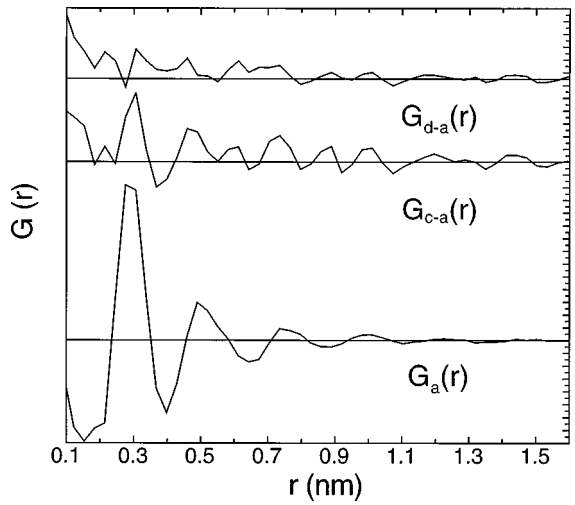

FIG. 5. Differences of RDF obtained after subtracting $G_a(r)$ from $G_c(r)$, $G_d(r)$. $G_{c-a}(r)=G_c(r)-G_a(r)$, $G_{d-a}(r)=G_a(r)-G_d(r)$.

MG of the precursor phase induced by crystallization. The curves of $G_{c-a}(r)$ and $G_{d-a}(r)$ have the same peak positions and shape. The peaks in $G_{c-a}(r)$ are relatively stronger compared with that of $G_{d-a}(r)$. This means that the crystallized specimen with preceding decomposition has a larger volume fraction of the crystalline phases in the MG.

IV. DISCUSSION

A. The relation between microstructural characteristics and GFA

Based on the above experimental and analytical results, we conclude that the bulk $Zr_{41}Ti_{14}Cu_{12.5}Ni_{10}Be_{22.5}$ MG has two microstructural characteristics that are distinct from the conventional MG: (1) The MG has a highly dense, randomly packed microstructure. (2) The MG shows significant differences in microstructure and composition compared to the corresponding crystalline compounds. The atomic structural characteristics should have close relation with the GFA of the MG. For the conventional MG, the second peak has a obvious splitting that indicates the difference of the local structure between the MG and its liquid states.[25] For the present RDF curve of the bulk MG, the second peak of the RDF curve has no obvious separation, which is analogous to that of a liquid. The difference is explained based upon the fact that the MG has a similar microstructure with its corresponding liquid state. The results demonstrate that the MG can truly be regarded as a glass formed continuously from its liquid state at a lower cooling rate: the local structure of the MG is more close packed than that of the conventional MG. The highly dense, randomly packed structure of the MG results from large atomic size ratios in the multicomponent. Be atoms with a much smaller atomic size relative to other constituents tighten the alloy structure and decrease the free volume and play a crucial role in the formation of this kind of microstructure. This is supported by our experimental results that show the GFA is sensitive to the Be content. The more close-packed structural characteristics of the MG cause the high viscosity in the supercooled liquid state and make the redistribution of atoms on a large range scale in the melt extremely difficult.

The local atomic configuration of short-range order in the conventional MG with no good GFA resembles the corresponding equilibrium compounds with a composition near that of the MG.[15,25–29] The similarity between the MG and crystalline phase (usually the Laves phase) is a fairly general microstructural characteristic of the early-transition-metal–late-transition-metal MG.[28] The compoundlike local structures in the MG make the crystallization usually close to a polymorphic crystallization. In contrast, the local atomic arrangement in the MG is markedly different from that of the corresponding crystalline compounds. The observed phase separation phenomenon in the MG indicates that a large composition difference exists between the MG and its corresponding crystalline compounds, because a decomposition takes places only in an alloy in which its composition is far away from the corresponding crystalline compounds.[30] So, there are no microstructural and compositional similarities between the MG and its corresponding crystalline compounds. A significant large SLR in the MG further confirms the structural characteristics. For conventional binary MG, ΔT is about 5 K, while for the $Zr_{41}Ti_{14}Cu_{12.5}Ni_{10}Be_{22.5}$ MG, $\Delta T=50$ K. The supercooled liquid state of the MG has a high resistance to nucleation and high stability in larger temperature ranges. This demonstrates that the nucleation and growth of the crystalline phases require substantial atomic diffusion, composition redistribution, high atomic mobility, and a larger time scale, even in the supercooled liquid state, and the MG has a much more compact structure and high viscosity in the supercooled liquid state. The two microstructural characteristics make the nucleation and growth of the crystalline phases from the initially homogenous supercooled liquid extremely difficult, because of the extremely slow mobility of the constituents in the high viscous supercooled liquid. It is very difficult for the five elements in the alloy to simultaneously satisfy the composition and structural requirements of the crystalline compounds. Therefore, the disordered liquid structure of the melt can be frozen with a low cooling rate, and then leads to a large GFA in the alloy system. The MG can be regarded as a true glass formed continuously from the melt liquid, and its local structure is then similar to the liquid. In fact, the GFA of such alloy system approaches that of the traditional oxide glasses. The origin for the excellent GFA of the MG results from the two microstructural characteristics.

The two microstructure characteristics result from the higher order multicomponent with very different atom size in the alloy system. As the number of components in a supercooled liquid is increased, the microstructure is more close packed, the composition deviation between the supercooled liquid and nucleation crystalline phase will be increased, and the nucleation and growth of the crystalline phase in the undercooled liquid state will be confused. This is the so-called ''confusion principle.''[31,32] Considering an alloy with n of equal concentration component elements, for $n=2$ to 10, the addition of each new element to the alloy will lower, by an order of magnitude, the probability of the composition fluctuation to achieving a critical nucleus.[32] In further support of this argument, carbon addition experiments on the $Zr_{41}Ti_{14}Cu_{12.5}Ni_{10}Be_{22.5}$ MG have been performed,[33] and reasonable agreement was found. A small amount of carbon addition further enhances the GFA and extends the SLR of

the MG, because carbon with a much smaller atomic size ($r_c = 0.091$ nm) further tightens the structure, decreases the free volume, and lowers the probability of the concentration fluctuation for crystalline formation in the melt. Carbon addition increases the degree of satisfaction for the confusion principle for achievement of a larger GFA.

It is likely that two microstructural characteristics are general structural characteristics for a multicomponent alloy system with excellent GFA. In fact, the high degree of dense random packing density local structure has been found in many multicomponent MG systems.[25] The large SLR of the MG originates from the two microstructure characteristics in the MG. This is supported by previous studies which confirm that the wide SLR has been generally found in other good glass forming alloy systems,[25,34] and the ΔT shows a good correlation with the GFA in the bulk MG.[1,25,34] In fact, it is evident that ΔT can be used to represent the GFA for the easy glass forming metallic alloys.[35] The reduced glass temperature T_{rg} defined by the ratio between T_g and the melting point temperature T_m,[36] which has been accounted for the GFA of the various conventional MG,[37] however does not reflect the relative GFA effectively among those good glass forming systems.[35] This further confirms that the microstructural difference exists between the bulk MG and the conventional MG. The good correlation between the larger SLR and the good GFA supports the view that the microstructural characteristics play a decisive role in the good GFA of the glass forming alloys.

B. The influence of the phase separation on the crystallization

The diffraction intensity analysis results demonstrate that the phase separation occurs in the $Zr_{41}Ti_{14}Cu_{12.5}Ni_{10}Be_{22.5}$ MG: the decomposed phases have different short-range orders and compositions compared to the MG. The decomposition destabilizes the MG and makes the MG thermally less stable with respect to crystallization. This conclusion is supported by experiments that show the relation of the thermal stability and the change of the Be content.[12,38] The results indicate that the thermal stability of the MG is increased by adding more Be. The Ti-rich Zr-Ti-Cu-Ni-Be MG is thermally less stable than the $Zr_{41}Ti_{14}Cu_{12.5}Ni_{10}Be_{22.5}$ MG. The experimental results support the suggestion that the decomposition destabilizes the MG and makes the MG thermally less stable with respect to crystallization, because the decomposed Ti-rich amorphous phase in the MG is thermally less stable than the MG and crystallizes in the lower temperature relative to MG. To clarify the phenomena, a schematic plot of the free-energy diagram is illustrated in Fig. 6, which exhibits schematically the decomposition and crystallization behaviors of the MG. The diagram can be read as a binary cut through a multicomponent alloy with respect to Be and Ti components in which the phase separation is involved. The free-energy curves for a supercooled liquid state of MG, two decomposed Be-rich and Ti-rich amorphous phases, and two crystalline compounds are drawn in the figure. As illustrated in the diagram, the MG can *go towards* the crystalline states in two crystallization paths. One process is the homogeneous nucleation of the crystalline compounds by a composition fluctuation directly from the initial homogeneous melt. Due to the microstructure and composition differences

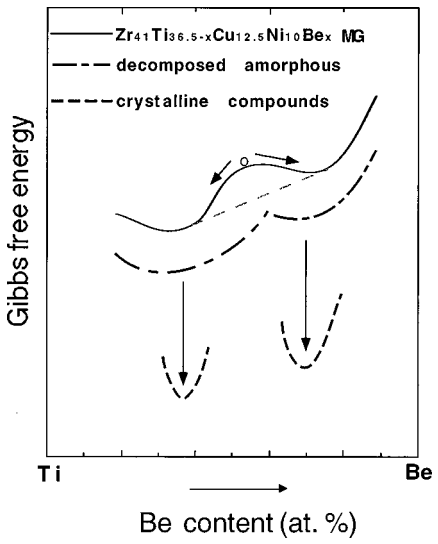

FIG. 6. Schematic Gibbs free energies of a supercooled liquid of the $Zr_{41}Ti_{14}Cu_{12.5}Ni_{10}Be_{22.5}$ alloy, two decomposed amorphous phases, and two crystalline compounds.

between the MG and its corresponding crystalline phases, the crystallization is a nonpolymorphic process. The MG can also undergo a preceding phase separation in SLR by spinodel decomposition and decomposes into two amorphous phases with no activation barrier: the decomposed phases have similar local structures and compositions to the respective crystalline compounds. Thus, the subsequent crystallization process is close to polymorphic. The two processes compete in the MG towards the crystalline state. The TEM observation and diffraction intensity analysis results demonstrate that the two crystallization phenomena do exist in the MG. To explain the crystallization phenomena kinetically, the activation barrier (ΔG^*) for the two nucleation process in the SLR of the MG is evaluated by $\Delta G^* = 16\pi\sigma^3/3(\Delta G)^2$, where ΔG is the chemical driving force for the formation of the crystalline phase, σ is the interfacial energy between liquid and crystal, which consists of a structural (σ^s) and a chemical contribution (σ^c),[39] $\sigma = \sigma^s + \sigma^c$ σ^s, σ^c result from the entropy difference across and the composition difference across the interface, respectively. In the polymorphic case, σ^c is very small because the composition difference across the interfaces can be neglected, and the nucleation barrier involving a composition fluctuation is very small, thus, the nucleation from the supercooled liquid state is a kinetically favored process in the polymorphic crystallization case (e.g., crystallization in conventional MG). For the nonpolymorphic crystallization of the MG, due to the larger compositional and local structural difference between amorphous and crystalline compounds, σ^s and σ^c are larger compared to the polymorphic case, and the nucleation barrier is much larger for nucleation of the crystalline phase directly from the homogeneous MG in a supercooled liquid: the nucleation needs a relative long-time scale and higher temperature. The phase separation makes the MG decompose into two amorphous phases that have similar composition and local structure to their respective crystalline compounds, and the subsequent crystallization close to the polymorphic process. The chemical contribution σ^c vanishing with the composition difference *across the amorphous*

and crystalline compound interface decreases, the structural contribution σ^s also decreases because of the similar local structure across the interface. Thus the nucleation barrier significantly decreases after the phase separation in MG, and the nucleation probability for the formation of the compounds in the decomposed phases increases compared to that in the initial MG. The phase separation may also give rise to a greatly decreased viscosity of the supercooled liquid and then increases the mobility of the atoms in the melt.[36] Meanwhile, the interfaces induced by decomposition promote the nucleation of the crystalline phases by providing the nucleation sites. So, the crystallization path through preceding decomposition is kinetically favored in the MG. The phase separation affects the subsequent crystallization by promoting the nucleation and decreasing the thermal stability of the MG. The existence of the phase separation tendency in the MG also reflects the large composition and local structure difference between the MG and its corresponding crystalline compounds.

V. CONCLUSION

Electron-diffraction analysis of the $Zr_{41}Ti_{14}Cu_{12.5}Ni_{10}Be_{22.5}$ MG as well as the decomposition and crystallization in the MG were performed. The MG is found to have a highly dense random-packed structure, which makes the redistribution of atoms on a large range scale extremely difficult in the supercooled liquid state. The large changes in $G(r)$ between the MG and its crystallized state demonstrate that the MG has a local structure that is far away from its corresponding crystalline compounds: the crystallization directly from the initial MG needs large scale range diffusion of the constituent atoms. The two microstructural characteristics of the MG, which are distinct from the conventional MG, retard the crystallization by suppressing nucleation and growth of the crystalline phase, and then lead to large GFA and wide SLR of the alloy. The phase separation in the supercooled liquid state is accompanied by a major structural rearrangement. The decomposed amorphous phases have close compositions and local structures to the respective crystalline compounds and exhibit a high nucleation rate in crystallization compared to that of the MG. The decomposition affects the subsequent crystallization by promoting the nucleation and destabilizing the thermal stability of the MG.

ACKNOWLEDGMENTS

The authors would like to thank Professor H. Wollenberger and Dr. L. Wanderka for their useful suggestions and discussions. W.H.W. is grateful for a grant from the Alexander von Humboldt Foundation in Germany.

*Author to whom correspondence should be addressed. Electronic address: whw@aphy02.iphy.ac.cn

[1] W. L. Johnson Mater. Sci. Forum **225-227**, 35 (1996).
[2] R. Busch, Y. J. Kim, and W. L. Johnson, J. Appl. Phys. **77**, 4039 (1995).
[3] A. Peker and W. L. Johnson, Appl. Phys. Lett. **63**, 2342 (1993).
[4] Y. J. Kim, R. Busch, W. L. Johnson, A. J. Rulison, and W. K. Rhim, Appl. Phys. Lett. **65**, 2136 (1994).
[5] R. Busch, Mater. Sci. Forum **235-238**, 327 (1997).
[6] U. Geyer, S. Schneider, W. L. Johnson, Y. Qin, T. A. Tombrello, and M. P. Macht, Phys. Rev. Lett. **75**, 2364 (1995).
[7] J. M. Liu, Mater. Sci. Eng. A **222**, 182 (1997).
[8] X. H. Lin and W. L. Johnson, J. Appl. Phys. **78**, 6514 (1995).
[9] M.-P. Macht, N. Wanderka, A. Wiedenmann, H. Wollenberger, Q. Wei, and H. J. Fecht, Mater. Sci. Forum **225-227**, 65 (1996).
[10] A. Wiedenmann, U. Keiderling, M.-P. Macht, and H. Wollenberger, Mater. Sci. Forum **225-227**, 71 (1996).
[11] M.-P. Macht, N. Wanderka, A. Wiedenmann, H. Wollenberger, Q. Wei, H. J. Fecht, and S. G. Klose, Mater. Res. Soc. Symp. Proc. **398**, 375 (1996).
[12] R. Busch, S. Schneider, A. Peker, and W. L. Johnson, Appl. Phys. Lett. **67**, 1544 (1995).
[13] S. Schneider, P. Thiyagarajan, and W. L. Johnson, Appl. Phys. Lett. **68**, 493 (1996).
[14] D. J. H. Cockayne and D. R. McKenzie, Acta Crystallogr., Sect. A: Found. Crystallogr. **44**, 870 (1988).
[15] M. A. Bursukova, E. P. Kashchieva, and Y. B. Dimitriev, J. Non-Cryst. Solids **192&193**, 40 (1995).
[16] M. Matsushita, Y. Hirotsu, K. Anazawa, T. Ohkubo, and T. Oikawa, Mater. Trans., JIM **36**, 822 (1995).
[17] N. Mori, T. Oikawa, T. Katoh, J. Miyahara, and Y. Harada, Ultramicroscopy **25**, 195 (1988).
[18] Q. Wei, Ph.D. thesis, Potzdam University, 1997.
[19] B. E. Warren, H. Krutter, and O. Morningstar, J. Am. Ceram. Soc. **19**, 202 (1936).
[20] T. Egami, Mater. Trans., JIM **31**, 163 (1990).
[21] S. G. Klose, Ph.D. thesis, Berlin Technical University, 1995.
[22] T. Zhang, A. Inoue, and T. Masumuto, J. Non-Cryst. Solids **156-158**, 473 (1993).
[23] A. Inoue, Mater. Trans., JIM **36**, 883 (1995); E. Matsubara, T. Tamura, Y. Waseda, T. Zhang, A. Inoune, and T. Masumoto, J. Non-Cryst. Solids **150**, 380 (1992).
[24] U. Gerold and H. Wollenberger (unpublished).
[25] Y. Waseda, *The Structure of the Non-crystalline Materials, Liquid and Amorphous Solids* (McGraw-Hill, New York, 1980).
[26] C. N. J. Wagner, J. Non-Cryst. Solids **150**, 1 (1992).
[27] R. Wang, Nature (London) **278**, 700 (1979).
[28] Sinkler, C. Michaelsen, and R. Bormann, Phys. Rev. B **55**, 2874 (1997).
[29] K. Suzuki, J. Phys.: Condens. Matter **3**, F39 (1991).
[30] W. Vogel, J. Non-Cryst. Solids **24**, 172 (1977).
[31] A. L. Greer, Nature (London) **366**, 303 (1993).
[32] P. J. Desre, Mater. Sci. Forum **179-181**, 713 (1995).
[33] W. H. Wang, Q. Wei, and H. Y. Bai, Appl. Phys. Lett. **71**, 58 (1997).
[34] A. Inoue, T. Zhang, and T. Masumoto, J. Non-Cryst. Solids **156-158**, 473 (1993).
[35] Y. Li, S. C. Ng, C. K. Ong, H. H. Hng, and T. T. Goh, Scr. Metall. Mater. **36**, 783 (1997).
[36] D. Turnbull, Contemp. Phys. **10**, 473 (1969).
[37] H. A. Davies, in *Rapidly Quenched Metals III*, edited by B. Cantor (The Metal Society, London, 1978), Vol. 1, p. 1.
[38] W. H. Wang and H. Y. Bai, J. Appl. Phys. (to be published).
[39] F. Spaepen, R. B. Meyer, Scr. Metall. **10**, 257 (1976).